Analytical Details

All analyses were performed at the Woods Hole Oceanographic Institution (USA). Micro-CT scans were performed using a tabletop Skyscan 1272 by Bruker. All peridotite cores were scanned using the same settings, before and after the hydrothermal experiments. Transmitted radiographs were collected at 0.34° steps over 180°. The source voltage was set at 90 kV with a current of 111 μA. An Al-Cu filter was used to reduce beam hardening artifacts. The pixel resolution ranged between 2.25 and 2.5 μm. The raw x-ray slices were reconstructed into cross-sections using Bruker NRecon software. Thermal misalignment correction, beam hardening artifact correction, ring artifact correction, and limited smoothing was applied to the data.

A Horiba Labram HR equipped with three lasers (473, 532, 633nm), two optical gratings (600 and 1800 grooves per mm), a motorized x-y-z stage, and an Olympus BX 41 petrographic microscope was used for confocal Raman analysis of minerals. Most Raman spectra were acquired with the red laser between 100 and 1280 cm^{-1}, with acquisition times varying between 5 and 20 seconds. To distinguish serpentine group minerals additional spectra were collected between 3500 and 3800 cm^{-1} for 10 to 30 seconds. Three to five accumulations were averaged per spot. The instrument is computer controlled with the LabSpec 6 Spectroscopy Suite software which was also used for post-acquisition processing of Raman spectra and comparison with reference spectra for mineral identification. The instrument is housed in a temperature-controlled environment and was calibrated daily using Ne and Ar emission lines. Most analyses were performed using a 100-X objective with a numerical aperture of 0.9 and achieved a spatial resolution better than 1 micrometer. The spectral resolution was better than 2 cm^{-1} and the repeatability was better than 0.02 cm^{-1}.

A TA Instruments Q-600 SDT instrument was used for thermogravimetric analysis and differential scanning calorimetry of partially serpentinized rocks. About 30 to 60 mg of powder were heated in N_2 with a flow rate of 50 milliliter per minute and a heating rate of 10 °C/min from room temperature to 1100 °C. The instrument was calibrated using weights supplied by the manufacturer and using the melting temperature of high purity standard materials. Acquired data were analyzed using the TA Instruments Universal Analysis software suite. Repeated analyses of reference materials were reproducible within ± 0.5 °C and 0.3 μg.

Determination of major dissolved elements was performed using a Thermo Scientific iCAP Qc inductively coupled plasma mass spectrometer in the Plasma Facility at the Woods Hole Oceanographic Institution. Samples were diluted (1000-fold) in high-purity deionized water (18.2 Ohm) to a final concentration of 2% HNO_3. Scandium, indium, and bismuth were added to each sample as an internal standard and HNO_3 blanks were run before and after the analyzed samples. Measurement uncertainties were 2% of the reported values.

Scanning electron microscopy (SEM) and energy-dispersive X-ray spectroscopy (EDS) were performed using a Hitachi TM3000 tabletop instrument equipped with a Bruker Quantax 70 EDS system on uncoated samples and thin sections. An acceleration voltage of 15 kV was used for all analyses.

Solid reactants and products

Solid starting materials from the Meerfelder Maar (Eifel area, Germany) were cut and drilled from the center of an unaltered harzburgite xenolith with a diameter of circa 30 cm. Subsamples of the same xenolith were used in a previous study (1) and the main characteristics are briefly repeated here. The harzburgite consists of olivine, orthopyroxene, clinopyroxene, and Cr-spinel, in addition to traces of amphibole, glass, pyrrhotite, and pentlandite. The diameter of primary minerals was <0.1 to 3mm (~1mm on average) and their compositions are reported elsewhere (1). The density of the harzburgite was 3.326g/cm^3 and loss on ignition was not detectable. Mössbauer spectroscopy revealed no ferric iron. All samples were moderately fractured and showed open pore space which has been interpreted to be due to decompression and thermal relaxation during rapid ascent of the xenolith(1). The modal proportions of primary minerals in cylindrical subsamples varied between orthopyroxene-rich harzburgite (n=4) and pyroxenite (n=1)

Solid starting materials from the Twin Sisters Massif (Washington, USA) were cut and drilled from a 20 x 20 x 10cm piece of unaltered pyroxene-poor harzburgite. The modal proportions of primary minerals in cylindrical subsamples varied between harzburgite (n=4) and dunite (n=2), and are directly comparable to previously reported modal abundances in ultramafic rocks from the same area (2). Notably, in comparison with cylindrical cores of rocks from the Eifel area, they contain more olivine and less pyroxene on a modal basis (Table S1). Grain sizes of primary minerals ranged from < 0.1 to circa 4mm; however, the average estimated grain size was larger (~2 mm) than that in rocks from the Eifel area. Compositions of primary minerals are reported elsewhere (2). Rocks were less fractured and less porous than those from the Eifel area.

Serpentinization of harzburgite and pyroxenite with molar olivine:orthopyroxene ratios of 0.5-1.4 (experiments # 01-06) resulted in the formation of serpentine (lizardite > chrysotile), talc, magnetite, and traces of chlorite in veins and pseudomorphic textures that mimic natural serpentinites (Fig. DR4). In experiments # 7-10, and 12, serpentinization of harzburgite and dunite with molar olivine:orthopyroxene ratios of 4.4-13.6 resulted in the formation of serpentine (lizardite > chrysotile), brucite, and magnetite in mesh texture and serpentine only in bastite texture (Figs. S1-S3). In addition to serpentine and brucite, alteration of harzburgite in experiment # 11 locally produced traces of talc where it formed at the expense of orthopyroxene together with serpentine.

Modal mineral proportions of solid reactants by micro-CT

Modal proportions were extracted from the 3-D scans of the protoliths. The thresholding of mineral phases with small density contrast (olivine, orthopyroxene, and clinopyroxene) was done using a combination of thresholding tools after all scans were corrected for beam hardening artifacts. All minerals phases were thresholded using the 3-D analysis software package Avizo®. Data were smoothed using a median filter. The olivine, orthopyroxene and clinopyroxene were thresholded using a combination of watershed and top-hat segmentation tool, while spinel was thresholded using a global threshold tool similar to what had been used in the CTAn software. The volume of each segmented material was subsequently computed.

Thermogravimetric analysis: Data analysis

The proportions of hydrous minerals and the extents of reaction were determined by thermogravimetric analysis (TGA). Hydrous minerals formed in experiments # 1-6 include serpentine (lizardite + chrysotile) and talc, as well as traces of chlorite, whereas hydrous minerals

formed in experiments # 7-12 include serpentine (lizardite + chrysotile) and brucite. Distinct thermal stabilities of these minerals were evident from weight loss, and the 1st derivative of the weight loss data (Fig. 4, Fig. S4). In experiments # 1-6 serpentine decomposition occurred in a temperature interval of 430 to 750 °C while talc decomposed between 750 and 900°C. In experiments # 7-12 serpentine decomposed between 450 and 715°C, whereas brucite decomposed between 250 and 450°C. Because the mass of OH lost from hydrous minerals, their mass can be directly calculated in each sample (Table DR1). The combined mass of hydrous minerals, minus their water content was used to calculate the extent of reaction in terms of wt.% protolith reacted (Table DR1). For simplicity, insignificant masses of Mg added and Ca lost during serpentinization were neglected. Volume changes in the reacted rock portions were computed by normalizing the volume change in the sample by the extent of reaction. The molar proportions of serpentine, talc, and brucite were used to calculate the molar proportions of olivine and orthopyroxene undergoing serpentinization, considering that Mg and Si were conserved in the rock (for simplicity, the addition of Mg from the fluid to the rock was neglected). The reacting molar proportions of olivine and pyroxene were used to compute relative olivine:orthopyroxene reaction ratios by comparison with molar (modal) proportions of these minerals in the protolith. The calculated results are consistent with thin section observations that orthopyroxene is more extensively altered than olivine. Concentrations of dissolved elements were used to assess to what extent they are mobilized from the reacting rock, by mass balancing them relative to those in secondary minerals (serpentine ~ $Mg_{2.85}Fe_{0.15}Si_2O_5(OH)_5$, brucite ~ $Mg_{0.9}Fe_{0.1}(OH)_2$, talc ~ $Mg_{2.85}Fe_{0.15}Si_4O_{10}(OH)_2$). Averaged rates of reaction were calculated by dividing the extent of alteration by the duration of the experiment in terms of wt.% per day. The surface areas of the minerals likely did not change to a significant extent, which is why it can be ignored in rate estimates provided here.
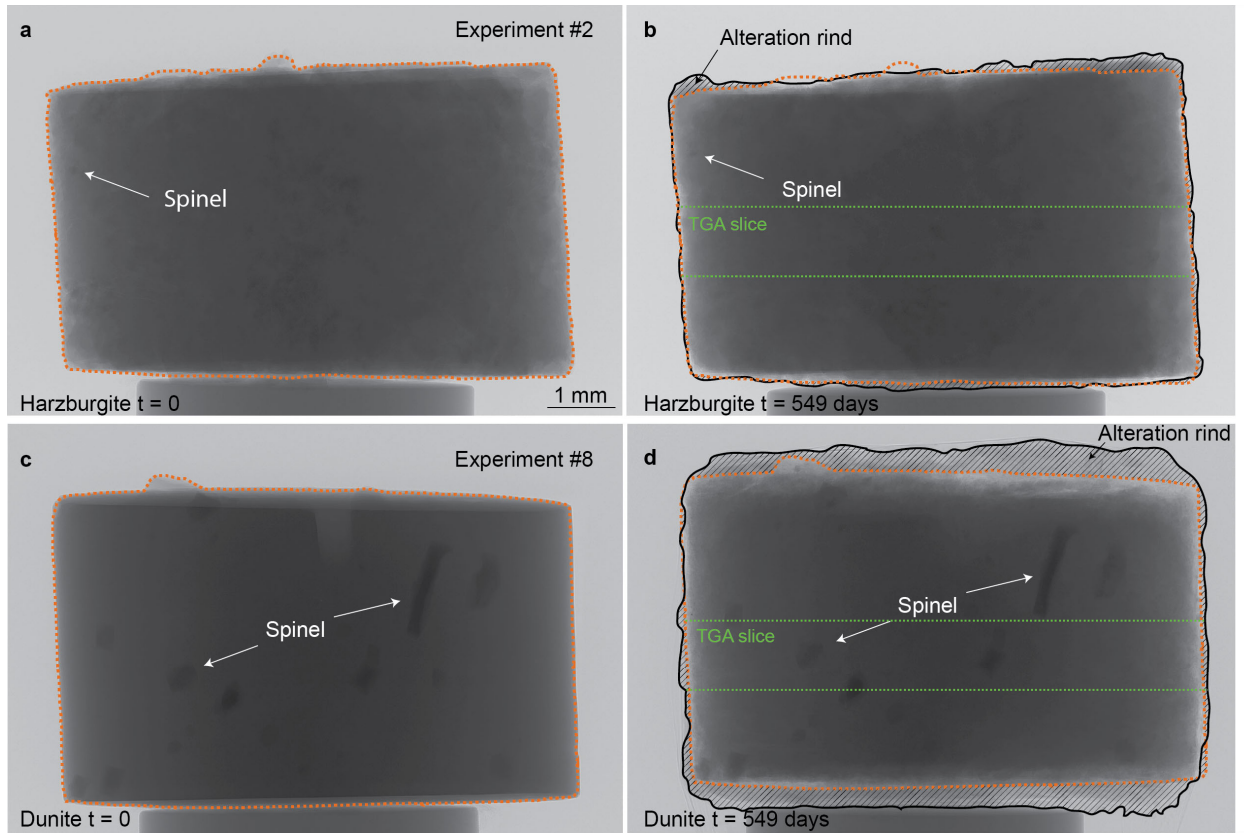
Fig. DR1. Micro-CT radiographs of rock cores before and after hydrothermal alteration. Orange dashed lines contour rock exterior before the experiments whereas solid black lines contour rock exteriors after the experiments. Hatched areas denote newly formed alteration rind. Green dotted lines indicate approximate location of rock slice cut for thermogravimetric analysis. (a) Fresh olivine-orthopyroxenite from the Eifel area used in experiment # 2., (b) Partially serpentinized olive-orthopyroxenite from experiment # 2. (c) Fresh harzburgite from the Twin Sisters Massif used in experiment # 8. (d) Partially serpentinized harzburgite from experiment # 8. Note that the scale is the same in all panels.
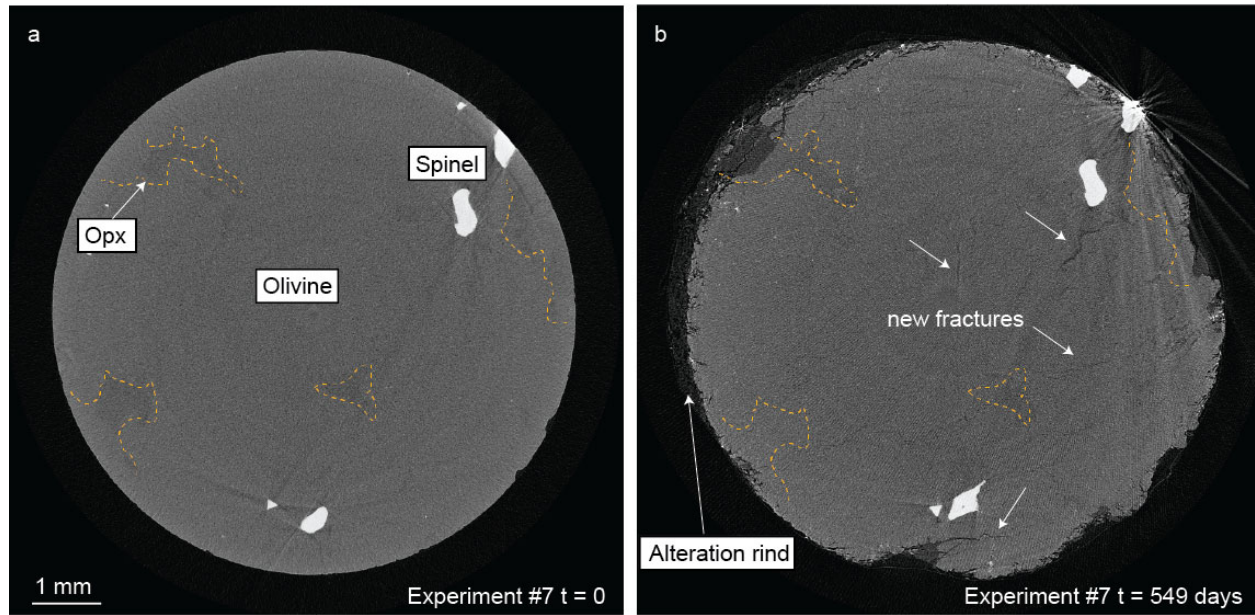
Fig. DR2. Micro-CT cross-section through experiment #7. (a) Unaltered harzburgitic protolith at t = 0 showing olivine and orthopyroxene-rich regions. (b) Comparable cross-section of the same harzburgite after 549 days of serpentinization. The core is surrounded by an alteration rind, orthopyroxene-rich regions show more reaction on average than olivine-rich regions, and new secondary mineral filled fractures have propagated into the core of the sample.
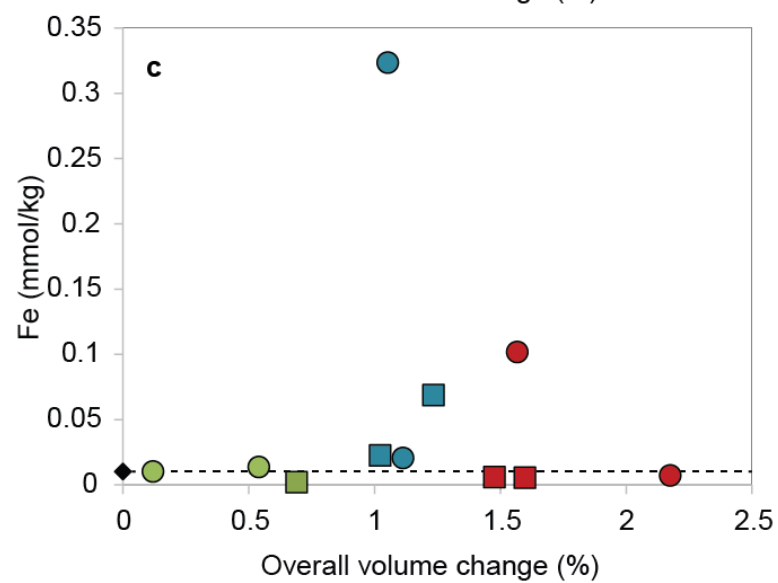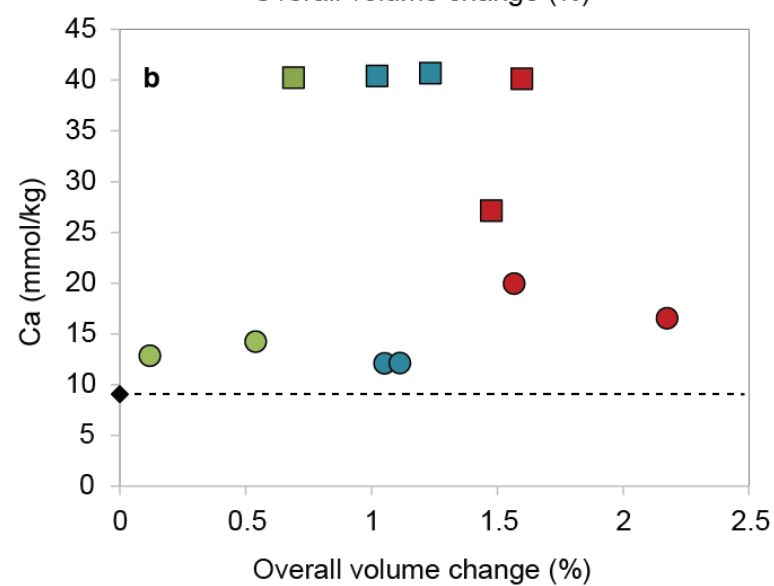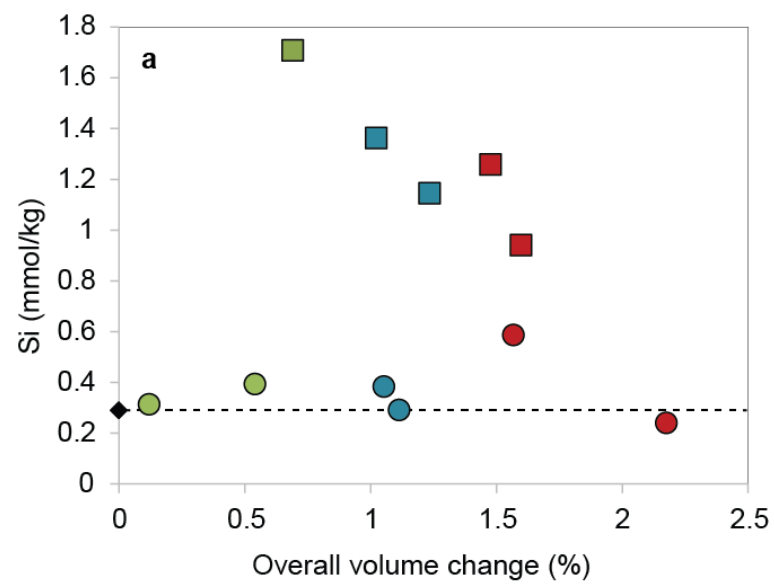
Fig. DR 3. Changes in fluid chemistry as a function of volume change. Horizontal dashed lines denote concentrations in starting solution. (a) Dissolved Si increased and then steadily decreased with increasing volume in experiments # 1-6 (Eifel). In contrast, in experiments # 7-12 (Twin Sisters) concentrations of dissolved Si did not change with volume. Overall, Si was conserved in the rock. (b) Dissolved Ca increased and then remained constant with increasing volume in experiments # 1-6. In experiments # 7-12 concentrations of dissolved Ca were higher than in the starting solution, but lower than in experiments #1-6. These patterns mirror those of dissolved Mg, suggesting linear exchange between Mg and Ca (see Fig. 3 in the main text). (c) Concentrations of dissolved Fe remained low in all but one experiment. Mass balance calculations suggest that more than 99% of the original Fe was conserved in the rock.
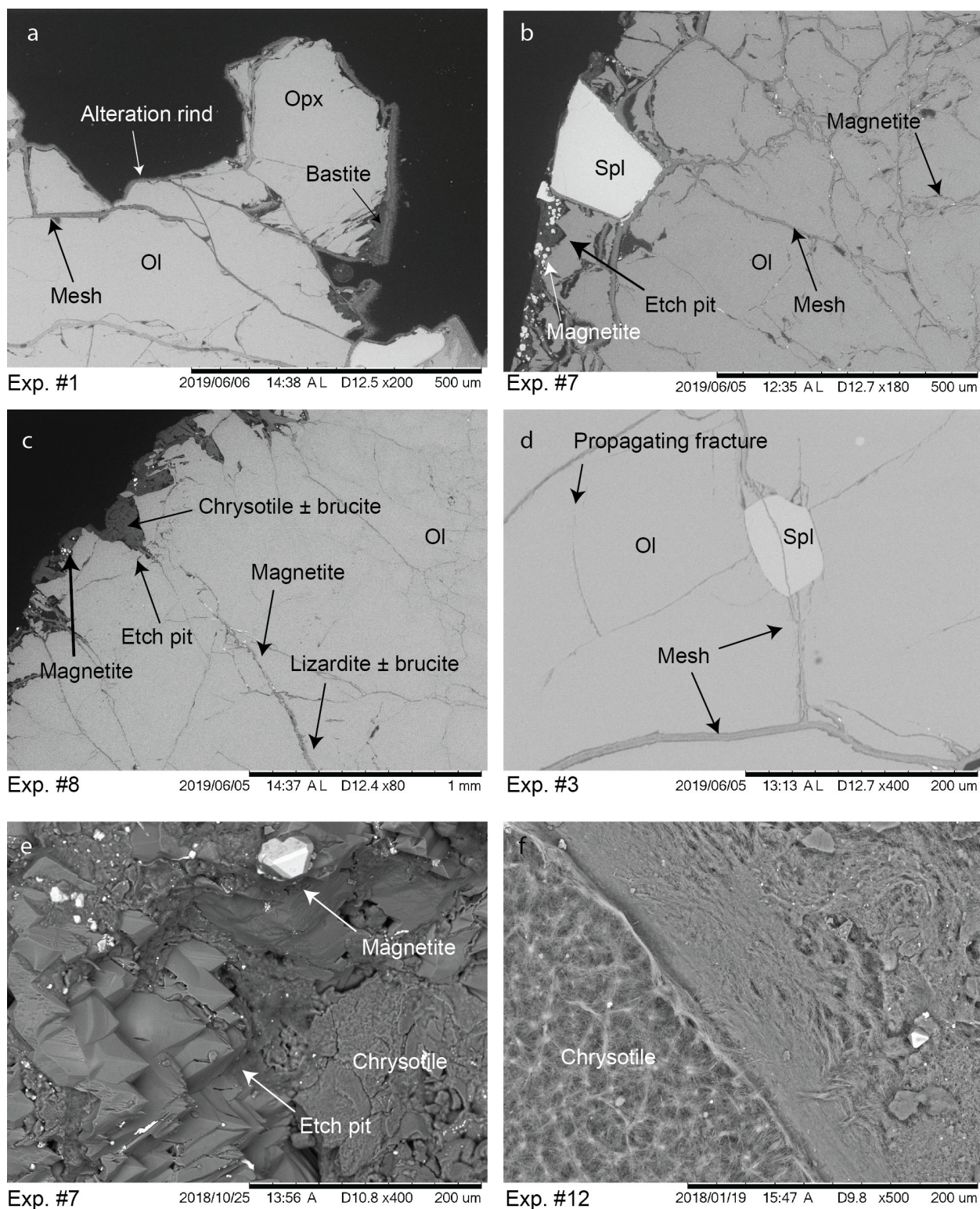
Fig. DR4. Back-scattered electron images of altered rocks from hydrothermal experiments in thin section (a-d) and rock surfaces (e-f). (a) Partially altered pyroxene-rich harzburgite. Alteration rinds around orthopyroxene are thicker than those around olivine suggesting preferential dissolution of orthopyroxene. Both mesh texture after olivine and bastite texture

after orthopyroxene primarily chiefly consist of serpentine. (b) Incipient mesh texture after olivine. Cone-shaped etch pits in olivine are filled with secondary minerals. and Magnetite formed together with chrysotile and brucite in mesh texture. Cr-spinel remained virtually unaltered. Note the abundance of veinlets inside the partially-altered core. (c) Incipient mesh texture after olivine in rock interior is composed of lizardite, brucite and traces of magnetite. The alteration rim formed at the expense of olivine consists of chrysotile, minor brucite, and magnetite. (d) Fractures in partially altered olivine and unaltered spinel (Spl) filled with secondary minerals. (e) Etch pits in olivine partially covered by chrysotile and magnetite. (f) Dense mats of chrysotile cover surface of partially altered dunite.
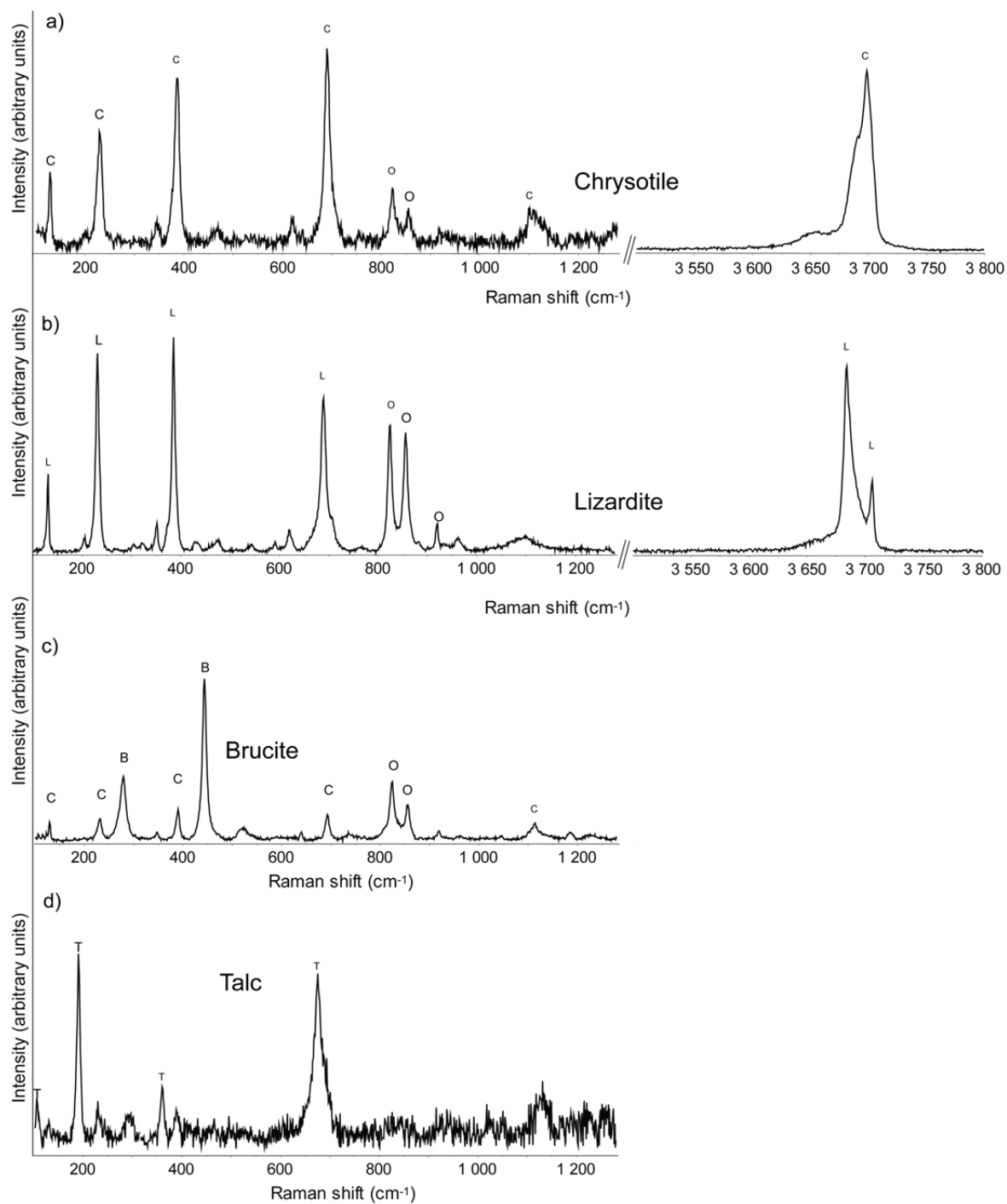
Fig. DR5. Representative Raman spectra of hydrous minerals formed during the experiments. (a) Chrysotile (abbreviated - C) after olivine, O. (b) Lizardite, L after olivine. (c) Brucite, B, and chrysotile after olivine. (d) Talc after orthopyroxene.

Table DR1: Characterization of solids

Experiment #	Rock type	Locality	Days of experiment	Volume change in reacted rock (%)	Overall extent of reaction (%)	Opx/Ol reaction rate	Reaction rate wt.% per day	Reaction products[1]
1	Harzburgite	Eifel, GE	320	58.7	2.10	1.87	6.57E-03	Srp, Tlc, Mag, ±Chl
2	Olivine orthopyroxenite	Eifel, GE	549	37.5	4.26	1.60	7.77E-03	Srp, Tlc, Mag, ±Chl
3	Harzburgite	Eifel, GE	549	54.3	2.72	1.84	4.96E-03	Srp, Tlc, Mag, ±Chl
5	Harzburgite	Eifel, GE	320	34.3	2.98	4.09	9.33E-03	Srp, Tlc, Mag, ±Chl
6	Harzburgite	Eifel, GE	144	29.7	2.33	2.84	1.62E-02	Srp, Tlc, Mag, ±Chl
7	Harzburgite	Twin Sisters, USA	549	39.8	5.47	2.01	9.96E-03	Srp, Brc, Mag
8	Harzburgite	Twin Sisters, USA	549	42.4	3.70	1.45	6.73E-03	Srp, Brc, Mag
9	Harzburgite	Twin Sisters, USA	144	23.6	2.29	1.47	1.59E-02	Srp, Brc, Mag
10	Dunite	Twin Sisters, USA	144	6.5	1.84	3.12	1.28E-02	Srp, Brc, Mag
11	Harzburgite	Twin Sisters, USA	320	42.4	2.48	2.80	7.76E-03	Srp, Brc, Mag
12	Dunite	Twin Sisters, USA	320	43.9	2.54	3.73	7.93E-03	Srp, Brc, Mag

[1]Srp = serpentine; Tlc = talc; Mag = magnetite; Chl = chlorite; Brc = brucite

Table DR2: *Concentrations of dissolved elements in mmol/kg (mM)*

Experiment #	Mg (mM)	Si (mM)	Fe (mM)	Ca (mM)	K (mM)	Na (mM)	Cl (mM)
1	7.12	1.14	0.069	40.7	3.76	438.52	NA
2	6.38	0.940	0.005	40.1	2.96	397.95	NA
3	21.5	1.3	0.006	27.1	1.67	392.79	NA
5	7.64	1.36	0.022	40.4	3.02	418.07	NA
6	11.2	1.71	0.002	40.2	2.64	443.25	NA
7	36.4	0.240	0.007	16.5	0.377	418.56	NA
8	30.7	0.587	0.102	19.9	0.398	426.30	NA
9	40.7	0.393	0.014	14.2	0.355	420.04	NA
10	44.0	0.313	0.010	12.8	0.363	418.76	NA
11	38.0	0.383	0.323	12.1	0.374	413.99	NA
12	44.1	0.291	0.021	12.1	1.00	407.60	NA
Starting fluid	48.8	0.286	0.005	9.05	0.293	397.07	464*

* calculated value, NA = not analyzed, uncertainties are 2% of the reported value